

# Thermal phase diagram of a model Hamiltonian for columnar phases of liquid crystals

M. Hébert\* and M. L. Plumer

*Centre de Recherche en Physique du Solide and Département de Physique, Université de Sherbrooke, Sherbrooke, Québec, Canada J1K 2R1*

(Received 1 September 1995)

We present the phase diagram and critical properties of a coupled  $XY$  Ising model on a triangular lattice using the mean-field approximation, the Migdal-Kadanoff renormalization-group scheme, and Monte Carlo simulations. The topology of the phase diagram is similar for the three techniques, with the appearance of a phase with  $XY$  order and Ising disorder. Critical exponents estimated from preliminary finite-size scaling are not inconsistent with Ising universality. This model is relevant to the columnar phases of discotic liquid crystals [such as hexa(hexylthio)triphenylene] in the limit of weak intercolumn coupling. [S1063-651X(96)03006-1]

PACS number(s): 61.30.Cz, 64.70.Md, 64.60.Ak, 75.10.Hk

## I. INTRODUCTION

Columnar phases of discotic liquid crystals are becoming a field of increasing experimental and theoretical activity in areas traditional to magnetic systems (modulated phases, stability, critical phenomena, etc.) [1,2]. Particular attention has been given to hexa(hexylthio)triphenylene (HHTT) compounds since they were found to be excellent photoconductors [3]. The photoinduced charge carrier mobility is four orders of magnitude higher than organic materials suitable for electronic devices and opens the way to improved conventional and novel applications. At present, our efforts are focused on the understanding of the positional and orientational orderings of the columnar phases.

The HHTT compound, first synthesized in 1984 [4], has been thoroughly studied by x-ray diffraction [5–8]. These measurements indicate that two intermediate columnar phases are present between the low-temperature crystalline  $K$  phase and the high-temperature isotropic liquid phase  $I$ . Upon cooling from the  $I$  phase, the system enters the disordered hexagonal  $D_{hd}$  phase at  $T \approx 93^\circ\text{C}$ , where the disklike molecules form columns, which are arranged on a triangular lattice. The  $D_{hd}$  phase is characterized by intracolumnar positional and orientational short-range order and long-range order in the triangular positions of the columns. As the temperature is reduced even further, the HHTT compound enters the ordered hexagonal columnar phase ( $H$  phase) at  $T \approx 70^\circ\text{C}$ . In this phase, the molecules within the columns show long-range positional and orientational order (resolution limited [7]) while maintaining the triangular arrangement of columns. Inside the columns, the molecules of  $D_3$  internal symmetry are equally spaced and rotated by an angle  $\alpha$  of approximately  $45^\circ$  along the column axes [Fig. 1(a)]. The columns can be either left handed or right handed. As noted by Fontes [5], these observations leave only three degrees of freedom for each column: the helicity of the column, the overall orientational phase angle of the column, and the

vertical displacement of the column. The proposed [8] structure of the  $H$  phase of HHTT is characterized by the formation of a  $\sqrt{3} \times \sqrt{3} R30^\circ$  superlattice [Fig. 1(b)] in the helicity pattern and vertical positions of the molecules described as follows. One-third of the columns are displaced by half an intracolumnar intermolecular distance in the  $\hat{z}$  direction (along the stacking axis). This is thought to be a mechanism to relieve part of the frustration due to steric hindrance. The displaced columns also have opposite helicity to the undisplaced ones.

Other experiments (Rayleigh scattering [9]) on similar compounds have served to elucidate the question of the stability [1] of the  $H$  phase. It is currently advocated that the  $H$  phase of HHTT is characterized by quasi-long-range order within the columns [10]. Orientational order in the low-temperature region of the  $H$  phase has been explored by ground-state calculations [11] and reproduces experimental observations [5].

A model has been proposed recently to reproduce the sequence of phases of the HHTT compound [12]. This simple model Hamiltonian incorporates, to a certain extent, what was noted by Fontes [5] and mentioned earlier. It is a generalization of a model introduced by Plumer *et al.* [13]. The columns are taken as rigid helices inscribed in a two-dimensional triangular array. The state of a column is determined by its helicity  $K_i$  (Ising-like variable) and a global phase angle  $\theta_i$  ( $XY$ -like variable). The vertical displacement of a column is then viewed as a change in the global phase angle  $\theta_i$ : the displacement of a column in the  $\hat{z}$  direction by half an intracolumnar intermolecular spacing is replaced by the addition of the angle  $\alpha/2$  to  $\theta_i$  [12]. This simplifying approximation neglects fluctuations in positional and orientational degrees of freedom of individual molecules and mimics the change in helicity of a column, which would result from a gradual unwinding of the helix, by a simple flip in the variable  $K_i$ . This model is thought to be valid in the strong intracolumn coupling limit of the exact interaction energy [11].

To second order in the moments of the mass density of the columns, the interaction energy of the system, coupling  $XY$  and Ising variables on a triangular lattice, is [12]

\*Present address: Laboratoire de Physique de la Matière Condensée, 11 place Marcelin-Berthelot, 75231 Paris Cedex 05, France.

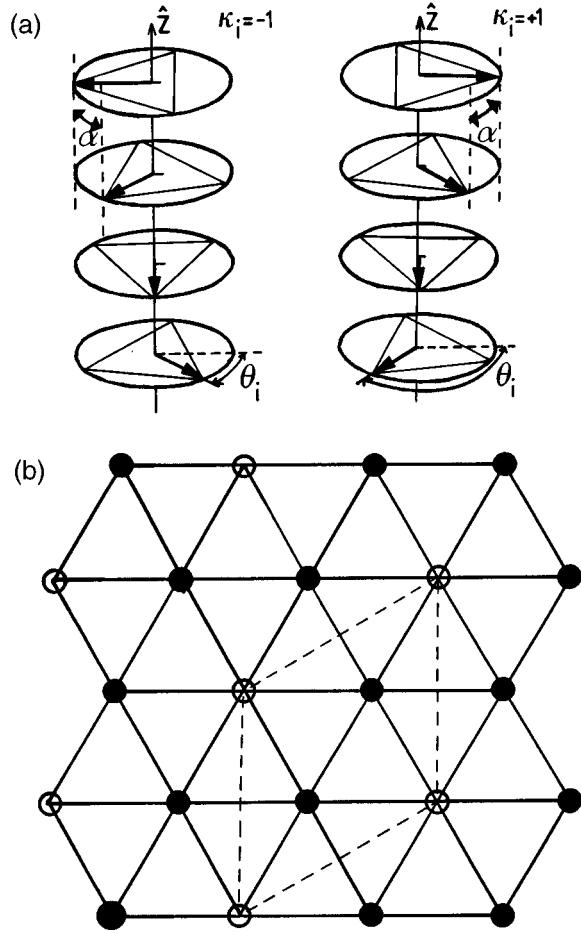


FIG. 1. (a) Schematic side view of a half period of HHTT in the  $H$  phase. The full period is composed of eight molecules of  $D_3$  internal symmetry symbolized by triangles. The two helicities  $K_i = \pm 1$  are represented. (b) Structure of the  $H$  phase in the basal plane showing the unit cell (dashed line). Displaced columns are represented by open dots and undisplaced columns by full dots.

$$\mathcal{H} = -\frac{J'}{2} \sum_{\langle ij \rangle} (1 + K_i K_j) \cos(\phi_i - \phi_j) - \frac{G'}{2} \sum_{\langle ij \rangle} (1 - K_i K_j) \cos(\phi_i + \phi_j), \quad (1)$$

with  $K_i = \pm 1$  and  $\phi_i = 3\theta_i$  ( $0 \leq \phi_i \leq 2\pi$ ). (We use primed parameters to be consistent with earlier calculations [12] and leave unprimed parameters for the exact interaction energy [11].) Note that the sign of  $G'$  is not relevant since changing  $G' \rightarrow -G'$  and  $\phi_i \rightarrow \phi_i + \pi/2$  leaves (1) invariant. This Hamiltonian with  $G' = 0$  has been studied extensively in relation to the fully frustrated XY models and Josephson junction arrays in a transverse magnetic field [14,15]. They reported a single continuous transition from an XY and Ising ordered phase to a totally disordered phase with exponents  $\nu = 0.83(4)$  and  $\beta/\nu = 0.14(2)$  associated with the Ising order parameter [16]. These results suggested the possibility of a new universality class. We note also that a similar model with no Ising variables [Hamiltonian (1) with  $K_i = K_j = 0$ ] has been studied recently [17].

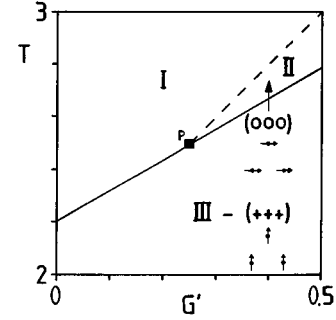


FIG. 2. Mean-field phase diagram of Hamiltonian (1) for  $J' = 1$ . Different phases are noted by roman numerals. Phase III is characterized by XY and Ising order, phase II by XY order with Ising disorder, and phase I by XY and Ising disorder. Helicity and angular configurations are represented and explained in the text. Solid and dashed lines represent first- and second-order phase transitions, respectively. The square denotes the location of critical end point.

It is also of interest to summarize briefly the intrinsic properties of Hamiltonian (1) in the low-temperature portion of the phase diagram [12]. For  $G' = 0$ , the effective exchange parameter for  $K_i K_j$  brings true long-range ferromagnetic order in the Ising variables, while the XY variables should exhibit Kosterlitz-Thouless order. For  $J' = 0$ , the effective exchange parameter for  $K_i K_j$  is antiferromagnetic. On a triangular lattice, this results in an Ising disordered state at all temperatures [18]. On the other hand, the term  $\cos(\phi_i + \phi_j)$  breaks the rotation invariance permitting true long-range order in the XY variables. The competition between the  $J'$  and  $G'$  terms is responsible for a rich  $T$ - $J'$  phase diagram within mean-field theory [12].

In this work, we study the  $T$ - $G'$  phase diagram and critical behavior of Hamiltonian (1) for  $J' = 1$ . In Sec. II the mean-field phase diagram (following [12]) is presented to give an indication of the type of order that may occur. In Sec. III we present the Midgal-Kadanoff renormalization-group study of Hamiltonian (1). Then, the phase diagram is calculated along with the critical exponents from preliminary Monte Carlo simulations (Sec. IV). Finally, general remarks and conclusions are drawn in Sec. V.

## II. MEAN-FIELD PHASE DIAGRAM

The mean-field phase diagram for  $G' = -1$  has already been published [12]. Here we use the same technique to calculate the  $J' = 1$  phase diagram ( $J' = 1$  fixes the energy scale). The main purpose of this calculation is to gain knowledge of the order parameters describing each phase. To sixth order in a Landau-type expansion of the free energy for a unit cell (see Ref. [12]), the resulting phase diagram is given in Fig. 2.

Despite the fact that the mean-field approximation is crude, a lot of information can be extracted from Fig. 2. The low-temperature phase (phase III) is characterized by XY and Ising order [ $\langle \phi_i \rangle = \langle \phi_j \rangle = \pi/2$  and  $(\langle K_1 \rangle \langle K_2 \rangle \langle K_3 \rangle) = (+++)$ ]. Phase II shows the existence of XY order with Ising disorder [ $\langle \phi_i \rangle = \langle \phi_j \rangle \neq 0$  and  $(\langle K_1 \rangle \langle K_2 \rangle \langle K_3 \rangle) = (000)$ ]. Finally, the high-temperature phase (phase I) has both XY and Ising disorder. As expected, for  $G' = 0$ , we

have a direct transition from phase III to phase I [14], but the order of the transition is wrong (see below) within the mean-field approximation. The  $G'$  term is responsible for the stabilization of phase II with  $XY$  order and Ising disorder. In fact, this phase II appears only for  $G' \geq 0.25$ . Note that italic letters ( $I$ ,  $D_{hd}$ , and  $H$ ) refer to phases reported experimentally in HHTT and roman numerals (I, II, and III) denote the phases in the present study.

### III. MIGDAL-KADANOFF RENORMALIZATION-GROUP APPROACH

In order to go beyond the Landau-type mean-field theory of Sec. II and include fluctuations of the order parameters, we apply the Migdal-Kadanoff renormalization-group scheme to a wider class of Hamiltonians

$$\beta\mathcal{H}_{\text{RG}} = -\frac{\beta J'}{2} \sum_{\langle ij \rangle} (1 + K_i K_j) \cos(\phi_i - \phi_j) - \frac{\beta G'}{2} \sum_{\langle ij \rangle} (1 - K_i K_j) \cos(\phi_i + \phi_j) - \frac{\beta L'}{2} \sum_{\langle ij \rangle} K_i K_j, \quad (2)$$

of which Hamiltonian (1) is the  $L'=0$  limiting case. The term  $-(\beta L'/2) \sum_{\langle ij \rangle} K_i K_j$  is added to (1) since its form is not preserved under renormalization (the renormalization process creates  $K_i K_j$  couplings). The Migdal-Kadanoff approach has been applied to Hamiltonian (2) with  $G'=0$  by a number of authors [14,19]. Those calculations were carried out on a square lattice with rescaling factors  $b=2$  and  $b=3$  in order to detect an antiferromagnetic Ising order at large and negative  $L'$ . The addition of the  $G'$  term on a triangular lattice, representing an intrinsic Ising frustration, is responsible for the apparition of a new phase characterized by  $XY$  order with Ising disorder and should be given special attention. For these reasons, we will calculate the phase diagram of (2), for  $G' < J'$ , using the Migdal-Kadanoff approximation implemented by Lee *et al.* [14], directly on the triangular lattice with a rescaling factor  $b=2$ .

To apply the Migdal-Kadanoff transformation, bonds are moved in such a way that half the sites (to be integrated out) are linked to only two neighbors (in one spatial direction). This bond moving leads to a one-dimensional decimation to obtain the effective exchange parameters between remaining sites. In terms of new variables  $u(\theta) = \exp[U(\theta) - U(0)]$ ,  $v(\theta) = \exp[V(\theta) - V(0)]$ , and  $z = \exp[U(0) - V(0) + \beta L']$  with  $U(\theta) = \beta J' \cos(\theta)$  and  $V(\theta) = \beta G' \cos(\theta)$ , the recursion relations are

$$\begin{aligned} [u'(\phi_1 - \phi_2)]^2 &= \frac{z^4 A_1(\phi_1 - \phi_2) + z^{-4} A_2(\phi_1 - \phi_2)}{z^4 A_1(0) + z^{-4} A_2(0)}, \\ [v'(\phi_1 + \phi_2)]^2 &= \frac{A_3(\phi_1 + \phi_2) + A_4(\phi_1 + \phi_2)}{A_3(0) + A_4(0)}, \\ [z']^2 &= \frac{z^4 A_1(0) z^{-4} A_2(0)}{A_3(0) + A_4(0)}, \end{aligned} \quad (3)$$

where

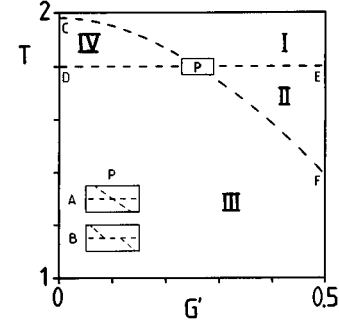


FIG. 3. Topological features of the phase diagram of Hamiltonian (2) within the Migdal-Kadanoff renormalization scheme for  $J'=1$  and  $L'=0$ . Phases are labeled as in Fig. 2, with phase IV representing  $XY$  disorder with Ising order. All transitions are continuous (dashed lines). The structure at point  $P$  cannot be determined accurately; the two possibilities are represented by the insets  $A$  and  $B$ .

$$A_1(\theta) = \int_0^{2\pi} \frac{d\bar{\phi}}{2\pi} u^4(\theta - \bar{\phi}) u^4(\theta),$$

$$A_2(\theta) = \int_0^{2\pi} \frac{d\bar{\phi}}{2\pi} v^4(\theta - \bar{\phi}) v^4(\theta),$$

$$A_3(\theta) = \int_0^{2\pi} \frac{d\bar{\phi}}{2\pi} u^4(\theta - \bar{\phi}) v^4(\theta),$$

$$A_4(\theta) = \int_0^{2\pi} \frac{d\bar{\phi}}{2\pi} v^4(\theta - \bar{\phi}) u^4(\theta). \quad (4)$$

The primed variables in (3) are the renormalized exchange parameters (after decimation) and should not be confused with  $J'$ ,  $G'$ , and  $L'$ , which are the coupling constants of the original Hamiltonian (2). In deriving (3), the only assumption on the potentials  $U(\theta)$  and  $V(\theta)$ , during the renormalization process, is their periodicities.

The phase diagram obtained by numerically iterating (3) is presented in Fig. 3 for  $J'=1$  and  $L'=0$ . It is comprised of four phases: I, a high-temperature disordered phase; II, a phase with  $XY$  order and Ising disorder; III, a low-temperature fully ordered phase; and IV, a phase with Ising order and  $XY$  disorder. The low-temperature phase III is characterized by  $XY$  and Ising order [ $\beta J' \rightarrow (\beta J')^*$ ,  $\beta G' \rightarrow (\beta G')^*$  with  $(\beta J')^* = (\beta G')^*$ , and  $\beta L' \rightarrow \infty$ ]. The Hamiltonian with  $\beta G'=0$  [14] is a stable limit under the renormalization-group transformations (3), as well as the  $\beta J'=0$  limit. Thus, in the  $\beta G'=0$  case, we get  $\beta J' \rightarrow (\beta J')^*$ ,  $\beta G' \rightarrow 0$ , and  $\beta L' \rightarrow \infty$ . The intermediate temperature phase II shows  $XY$  order with Ising disorder [ $\beta J' \rightarrow (\beta J')^*$ ,  $\beta G' \rightarrow (\beta G')^*$  with  $(\beta J')^* = (\beta G')^*$ , and  $\beta L' \rightarrow 0$ ]. The  $PF$  line (Fig. 3) corresponds to an Ising-like transition within this approximation. In fact, putting  $(\beta J')^* = (\beta G')^*$  in (3) and (4), we find  $A_i^*(0) = A_j^*(0)$  and

$$[z']^2 = \frac{z^4 + z^{-4}}{2}, \quad (5)$$

which is the Migdal-Kadanoff recursion relation for the spin-1/2 Ising model with  $b=2$ . The *CPE* line is relatively difficult to locate due to the high-temperature drift suffered by the Migdal-Kadanoff approximation. The other intermediate-temperature phase IV is characterized by Ising order with *XY* disorder ( $\beta J' \rightarrow 0$ ,  $\beta G' \rightarrow 0$ , and  $\beta L' \rightarrow \infty$ ). This phase is not seen in the mean-field approach and we argue that it is an artifact of the renormalization-group scheme. The *PD* line cannot be located precisely since the Migdal-Kadanoff approach does not reproduce a line of true fixed points for the *XY* model. Nevertheless, this scheme generates a line of almost fixed points that gives a hint of *XY*-like ordered phases. Finally, because of these shortcomings of the Migdal-Kadanoff approximation, the exact topology of the bifurcation point *P* (insets *A* and *B* of Fig. 3) cannot be resolved.

As can be observed in Fig. 3, every phase transition is second order. The technique used to arrive at this conclusion is a generalization of the procedure known to reproduce the

first-order transition of the  $q$ -state Potts model for  $q > 4$  [20]. Our specific implementation is due to Lee *et al.* [14]. The idea is to have vacancies to prevent overestimation of the local order in the system.

The lattice-gas version of (2) reads

$$\begin{aligned} \beta \mathcal{H}_{\text{LG}} = & -\frac{\beta J'}{2} \sum_{\langle ij \rangle} (1 + K_i K_j) t_i t_j \cos(\phi_i - \phi_j) \\ & -\frac{\beta G'}{2} \sum_{\langle ij \rangle} (1 - K_i K_j) t_i t_j \cos(\phi_i + \phi_j) \\ & -\frac{\beta}{2} \sum_{\langle ij \rangle} (L' K_i K_j t_i t_j + K' t_i t_j) + \Delta \sum_i t_i, \end{aligned} \quad (6)$$

where the vacancy variable is  $t_i = 0, 1$  and  $\Delta$  is the fugacity. Applying the same renormalization scheme to (6), with  $w = \exp[K' + V(0) + U(0)]$  and  $y = \exp(\Delta)$ , we get the recursion relations

$$\begin{aligned} [u'(\phi_1 - \phi_2)]^2 &= \frac{2 + [z^4 A_1(\phi_1 - \phi_2) + z^{-4} A_2(\phi_1 - \phi_2)] w^4 y^{-2/3}}{2 + [z^4 A_1(0) + z^{-4} A_2(0)] w^4 y^{-2/3}}, \\ [v'(\phi_1 + \phi_2)]^2 &= \frac{2 + [A_3(\phi_1 + \phi_2) + A_4(\phi_1 + \phi_2)] w^4 y^{-2/3}}{2 + [A_3(0) + A_4(0)] w^4 y^{-2/3}}, \\ [w']^2 &= \frac{w^8 y^{8/3} \{2 + [z^4 A_1(0) + z^{-4} A_2(0)] w^4 y^{-2/3}\} \{2 + [A_3(0) + A_4(0)] w^4 y^{-2/3}\}}{2 w^{-2} y^{2/3} + B_1 z^2 + B_2 z^{-2}}, \\ y' &= \frac{w^{-12} y^6}{2 w^{-2} y^{2/3} + B_1 z^2 + B_2 z^{-2}}, \\ [z']^2 &= \frac{2 + [z^4 A_1(0) + z^{-4} A_2(0)] w^4 y^{-2/3}}{2 + [A_3(0) + A_4(0)] w^4 y^{-2/3}} \end{aligned} \quad (7)$$

with

$$\begin{aligned} B_1 &= \int_0^{2\pi} \frac{d\bar{\phi}}{2\pi} u^4(\bar{\phi}), \\ B_2 &= \int_0^{2\pi} \frac{d\bar{\phi}}{2\pi} v^4(\bar{\phi}). \end{aligned} \quad (8)$$

The  $\Delta t_i$  term has been distributed equally between bonds at site  $i$  before moving them. This is necessary to preserve the site density at each step of the renormalization process. The line of discontinuity fixed points, signaling the first-order transition, appears for  $w, y, z \rightarrow \infty$  [14,21]. In this limiting case, an almost fixed line appears when

$$y' [w']^{-2} [z']^2 = \frac{y^{14/3} w^{-12} z^{-12}}{A_1^*(0)^2}. \quad (9)$$

The criterion to have a discontinuity fixed point (corresponding to a first-order transition) states that eigenvalue  $\lambda$ , for

small deviations from the fixed point along the unstable direction, must be given by  $\lambda = b^d$  ( $d$  is the dimensionality of the lattice) [21]. We can see, from (9), that this is certainly not the case. Therefore, within the Migdal-Kadanoff approximation and using the procedure of Nienhuis and Nauenberg [21], the transitions in Fig. 3 are continuous.

It is of interest to compare our results with those of Lee *et al.* [14] in the limit of  $G' = 0$  and  $L' = 0$ . Within the Migdal-Kadanoff approximation, both calculations give the sequence of phases III  $\leftrightarrow$  IV  $\leftrightarrow$  I with second-order transitions between them.

#### IV. MONTE CARLO SIMULATIONS

In this section we report the results of a preliminary Monte Carlo study of the phase diagram and critical behavior of the model (1). We used the traditional Monte Carlo technique to locate the phase boundaries and to verify the overall temperature behavior of the thermodynamic quantities, especially the order parameters and susceptibilities. Then we used the Monte Carlo histogram technique to locate accu-

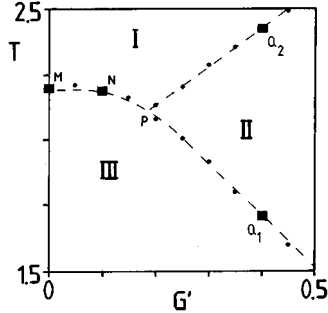


FIG. 4. Monte Carlo phase diagram, with  $J'=1$ , for a system size of  $36^2$  sites. Different phases are represented as in Fig. 2. Full circles denote the transition temperatures for a given  $G'$ . All transitions are continuous. Full squares and capital letters refer to the transitions where finite-size scaling was performed.

rately the transition temperatures and to estimate critical exponents by finite-size scaling analysis. Both Monte Carlo approaches used a sequential version of the Metropolis algorithm to test separately the Ising and XY trial configurations. A Monte Carlo step (MCS) is as follows. For each lattice site, the Metropolis test is applied to the Ising variable ( $K_i$ ) and then to the XY variable ( $\phi_i$ ).

#### A. Monte Carlo phase diagram

Figure 4 shows the resulting Monte Carlo phase diagram. It has been obtained for a  $L \times L$  lattice ( $L=36$ ) with  $10^5$  MCS for thermalization and  $4 \times 10^5$  MCS for averaging. We use the same convention as in the mean-field (Sec. II) and renormalization-group (Sec. III) phase diagrams to name the phases (roman numerals). To describe the order present in each phase, we define the order parameters

$$P_K = \left| \frac{1}{L^2} \sum_i K_i \right|, \quad (10)$$

$$P_{Mj} = \left| \frac{3}{L^2} \sum_{i \in \mathcal{S}_j} \vec{S}_i \right|, \quad (11)$$

where  $\mathcal{S}_j$  denotes one of the three sublattices and  $\vec{S}_i = (\cos(\phi_i), \sin(\phi_i))$  are pseudospin variables. The three XY-like  $P_{Mj}$  order parameters are very sensitive to sublattice switching. We therefore performed the simulations with the XY order parameter

$$P_M = \max_j (P_{Mj}), \quad (12)$$

which has a smoother temperature dependence than  $P_{Mj}$ . In order to understand each phase in Fig. 4, we present the order parameters  $P_K$  and  $P_M$  as functions of temperature [Fig. 5(a)]. Phase III ( $P_M$  and  $P_K \neq 0$ ) is the phase with XY and Ising order. The intermediate phase II keeps the XY order ( $P_M \neq 0$ ) but loses the Ising order ( $P_K = 0$ ). At high temperatures, the isotropic phase I has XY and Ising disorder ( $P_M$  and  $P_K = 0$ ). A behavior similar to that of the XY order parameter  $P_M$  and its susceptibility  $\chi_M$  [Fig. 5(b)]

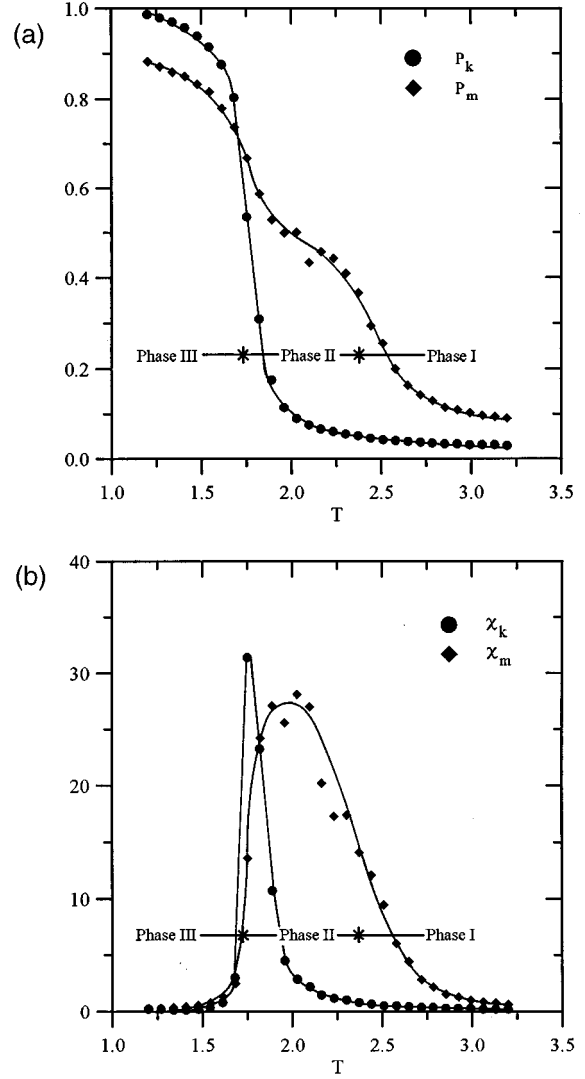


FIG. 5. (a) Temperature dependence of the Ising ( $P_K$ ) and XY ( $P_M$ ) order parameters for  $G'=0.4$ . (b) Temperature dependence of the susceptibilities associated with  $P_K$  and  $P_M$ .

in the phase II has been reported for the six-state clock model [23] and is characteristic of systems with intrinsic disorder.

The general features of the Monte Carlo phase diagram can be understood easily. For  $G'=0$ , there is a single transition from phase III directly to phase I [15]. This can be seen by noting that the mechanism required to have a transition in the Ising variables is the appearance of domain walls. For  $G'=0$ , at such a domain wall, the XY variables are decoupled since  $(1 + K_i K_j) = 0$ . In this case, Ising disorder induces XY disorder. On the other hand, for  $G' \gg J'$ , there should be no Ising order in the system (Sec. I). This is seen in Fig. 4: the  $P_{Q_1}$  line of transitions goes toward  $T=0$  as  $G'$  gets larger. Ultimately, for  $G' \rightarrow \infty$ , there is only one transition from a phase with XY order and Ising disorder to the phase I.

#### B. Finite-size scaling

The rest of this section is concerned with the finite-size scaling at the four points ( $M$ ,  $N$ ,  $Q_1$ , and  $Q_2$ ) shown in Fig.

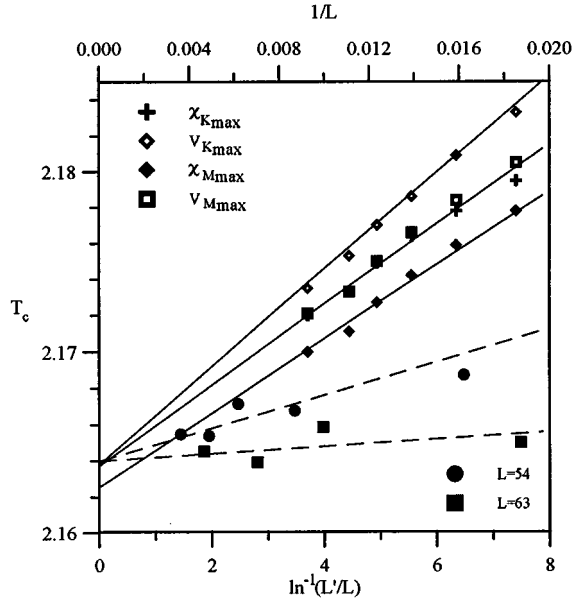


FIG. 6. Estimation of  $T_c$  for  $G'=0$ . The solid lines show the scaling of the extrema of  $\chi_K$ ,  $V_K$ ,  $\chi_M$ , and  $V_M$  vs  $L^{-1}$ . The dashed lines represent the scaling of  $T_c$  with respect to  $\ln^{-1}(L/L)$  using the cumulant-crossing method.

4. The goal here is to extract only rough estimates of the critical exponents. We are also interested in detecting the order of the transitions. Finite-size scaling using the Monte Carlo histogram method has been recently reviewed by Plumer *et al.* [24]. In our case, it involves the specific heat ( $C_v$ ), the energy cumulant ( $U_e$ ), the order parameters ( $P_M$  and  $P_K$ ), their susceptibilities ( $\chi_M$  and  $\chi_K$ ), their logarithmic derivatives ( $V_M$  and  $V_K$ ) [25], and their fourth-order cumulants ( $U_M$  and  $U_K$ ) [26]. We performed a simulation for each lattice size  $L=54, 63, 72, 81, 90$ , and 108 at our best estimate of the transition temperature  $T_0$  from the results for the order parameters, as in Fig. 5. Typically,  $(2-3) \times 10^5$  MCS were used for thermalization and  $(6-10) \times 10^5$  MCS were kept for averaging. Since we did only one simulation per lattice sizes at  $T_0$ , the error bars on the exponents are likely quite large (typically 10–15 %).

Let us focus on the transition  $M$ , at  $G'=0$ , where  $T_0=2.175$  in Fig. 4, to explain the details of the scaling analysis used here and because these results will be compared with data published earlier [15]. The well-studied fully frustrated XY model is also closely connected with Hamiltonian (1) with  $G'=0$  [22].

To determine the critical temperature  $T_c$ , we used the scaling with  $L^{-1}$  (which assumes  $\nu=1$ ) of the positions of the extrema of the susceptibilities ( $\chi_M$  and  $\chi_K$ ) and of the logarithmic derivatives ( $V_M$  and  $V_K$ ). In the special case of  $G'=0$ , the cumulant-crossing method (using  $U_K$ ) was also applied to get a better estimate of  $T_c$  [25]. The results are summarized in Fig. 6. Both techniques give roughly the same  $T_c$ . The scaling of the extrema of  $\chi_M$  and  $V_M$  gives  $T_{c-M}=2.1631(10)$ , while the scaling for  $\chi_K$  and  $V_K$  gives  $T_{c-K}=2.1635(7)$ . Using the cumulant crossing we get  $T_{c-CC}=2.1644(10)$ . From our data we can conclude that, given the errors on the critical temperatures, the transitions involving the XY-type and Ising-type order parameters occur

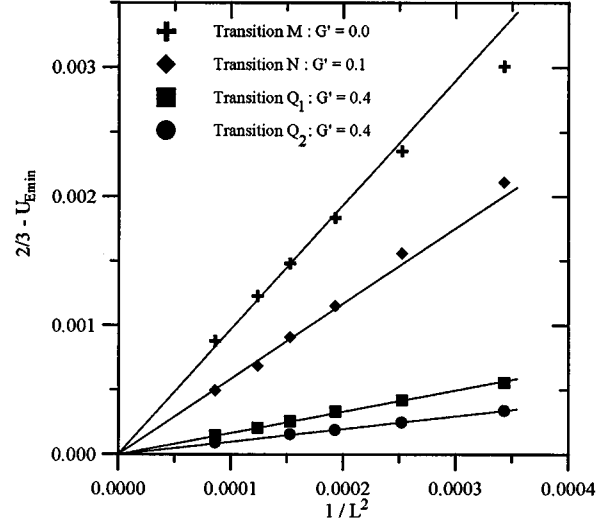


FIG. 7. Scaling of the minimum of the energy cumulant for the four transitions considered. Solid lines are guides to the eye.

at the same temperature, as expected [22,15]. The precision is quite good, especially when it is compared to the estimation of  $T_c$  in other systems [28,29]. The value of  $T_c$  is required to find  $\beta/\nu$  because  $P_K \sim L^{-\beta/\nu}$  at  $T_c$ . The other exponents can also be found by a scaling at  $T_c$ , but in our case the scaling of the extrema of the thermodynamical quantities proved to be more precise.

The size dependence of the minimum of the energy cumulant ( $U_e$ ) is given in Fig. 7 for the four transitions. The fact that  $U_e \rightarrow 2/3$  when  $L \rightarrow \infty$  indicates that the four transitions are continuous [30]. This is in agreement with our renormalization-group results (Sec. III) and with the results of Granato *et al.* [15] in the case of  $G'=0$ .

Figures 8 and 9 show the scaling that leads to the critical exponents  $\nu_K$  and  $\beta_K/\nu_K$  associated with the Ising order parameter  $P_K$ . In the case of  $\beta_K/\nu_K$ , we used the critical temperature given by the scaling of the extrema of  $\chi_K$ ,  $V_K$ ,  $\chi_M$ , and  $V_M$ . The rough estimates are  $\nu_K=1.1(1)$  and  $\beta_K/\nu_K=0.18(1)$ . The errors on the exponents are estimated only by the goodness of the fit on the plots and do not account for the (unknown) statistical error for each run. From

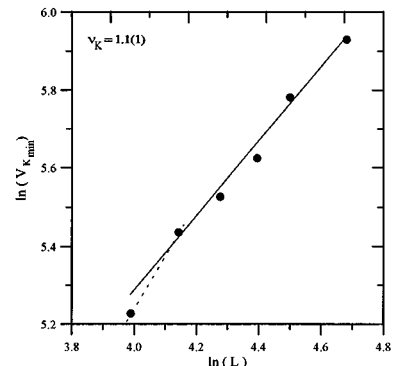


FIG. 8. Scaling of the logarithmic derivative of  $P_K$ . The solid line through the five largest lattice sizes gives the exponent  $\nu_K=1.1(1)$ . The dotted line is for the scaling using the two smallest lattice sizes (see the text).

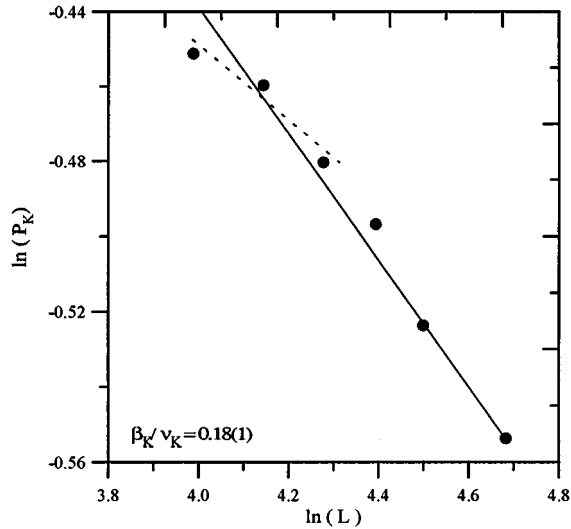


FIG. 9. Scaling of the order parameter  $P_K$  at  $T_c=2.1635(7)$ . The solid line through the five largest lattice sizes gives the exponent  $\beta_K/\nu_K=0.18(1)$ . The dotted line is for the scaling using the three smallest lattice sizes (see the text).

the relatively large scatter of the points on those figures, it appears that there are large statistical fluctuations. Our estimates of the exponents are in apparent disagreement with those of Granato *et al.* [15]. Their study involved very long Monte Carlo runs, but on relatively small lattice sizes ( $L \leq 40$ ). Scaling with only our three smallest lattice sizes ( $L=54, 63$ , and  $72$ ) gives  $\nu_K \approx 0.74$  and  $\beta_K/\nu_K \approx 0.10$ , which are closer to their results. It is clear that there are significant finite-size effects. Figure 10 presents the scaling of  $\chi_{K\max}$  with  $L$ , giving  $\gamma_K/\nu_K=1.55(16)$ .

These exponents ( $\nu_K$ ,  $\beta_K/\nu_K$ , and  $\gamma_K/\nu_K$ ) are not too different from those of the two-dimensional (2D) Ising universality class ( $\nu_K=1$ ,  $\beta_K/\nu_K=0.125$ , and  $\gamma_K/\nu_K=1.75$ ). In this case, the specific heat diverges like the logarithm of  $L$ . Figure 11 shows  $C_{v\max}$  against  $\ln L$ . The straight line fit for  $L \geq 63$  is an indication that, contrary to what was suspected earlier [15], the transition at  $G'=0$  may be of the 2D Ising universality class. Such logarithmic divergence of  $C_{v\max}$  for the infinite lattice is also reported for the fully frustrated XY model [27]. Extensive Monte Carlo simula-

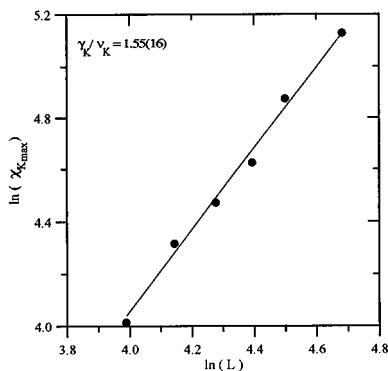


FIG. 10. Scaling of the susceptibility associated with  $P_K$ . The solid line through the five largest lattice sizes gives the exponent  $\gamma_K/\nu_K=1.55(16)$ .

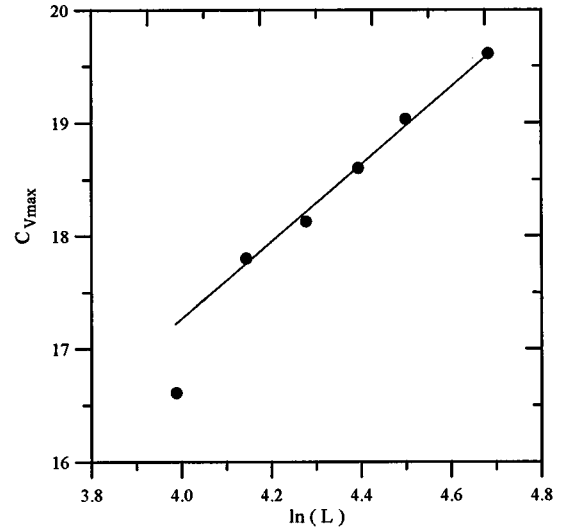


FIG. 11. Specific heat as a function of lattice size  $\ln(L)$ .

tions involving large lattice sizes and better statistics are required to verify this conclusion.

Table I lists the exponents for the four transitions considered, along with  $T_0$  and  $T_c$ . The missing values for the exponents at points  $Q_1$  and  $Q_2$  reflect the fact that for  $G'=0.4$ , the transitions involve only Ising and XY order, respectively. The errors on the exponents are estimated only by the goodness of the fit. The exponent  $\alpha=0$  (log) means that  $C_{v\max} \sim \ln(L)$ , as in the 2D Ising model. We note that  $\gamma_M/\nu_M$  at  $G'=0.4$  was estimated at  $T_c$ , because  $\chi_M$  shows only a broad maximum across the phase II and not a sharp peak [see Fig. 5(b)]. It was impossible to get an estimate of  $\beta_K/\nu_K$  for transition  $Q_1$ , the data being too erratic.

Under the assumption that for  $G'=0.0$  (and  $G'=0.1$ ) there is only a single transition, there can be only one characteristic length that diverges. The exponents  $\nu_K$  and  $\nu_M$  are related to the divergence at  $T_c$  of the Ising-type and XY-type correlation lengths, respectively. Thus  $\nu_K$  has to be equal to  $\nu_M$ , if there is a direct transition from phase III to phase I. This seems to be the case given the accuracy of our results. As noted in Ref. [14], however, the Ising and XY transitions may be decoupled if  $\nu=1$ . This question has also been addressed in relation to the antiferromagnetic XY model on a stacked triangular lattice [28].

Except for the values of  $\beta_K/\nu_K$  at points  $N$  and  $Q_1$ , from the data given in Table I and Fig. 7, we tentatively suggest that the transitions along the  $MPQ_1$  line are continuous and might belong to the 2D Ising universality class. This in agreement with our renormalization-group treatment of model (1) along the  $PF$  line of Fig. 3 in Sec. III. As for the other exponents,  $\gamma_K/\nu_K$  and  $\gamma_M/\nu_M$  seem to be stable along the  $MPQ_1$  line and may also suggest the 2D Ising universality class. However, the data for  $\beta_K/\nu_K$  and  $\beta_M/\nu_M$  are very noisy (see Fig. 9) and no definite conclusions can be drawn.

The last transition studied ( $Q_2$ ) is characterized by the loss of XY order while the Ising variables are disordered. The specific heat scaling shows no dependence on lattice size, indicating that  $\alpha \approx 0$ . A similar behavior has been observed in frustrated antiferromagnetic XY models in a mag-

TABLE I. Summary of the critical exponents for the four transitions considered. The errors are estimated by the robustness of the fit of the data and can be larger due to statistical fluctuations. The transitions  $Q_1$  and  $Q_2$  involve  $XY$  and Ising orders, respectively, and only those exponents are given. Question marks indicate large scatter in the data.

Exponent	$G' = 0.0$ ( $M$ )	$G' = 0.1$ ( $N$ )	$G' = 0.4$ ( $Q_1$ )	$G' = 0.4$ ( $Q_2$ )
$T_0$	2.175	2.165	1.745	2.37
$T_c$	2.1635(7)	2.148(2)	1.737(3)	2.376(5)
$\nu_K$	1.1(1)	1.18(16)	1.06(12)	
$\beta_K/\nu_K$	0.18(1)	0.57(1)?		
$\gamma_K/\nu_K$	1.55(16)	1.58(16)	1.64(16)	
$\nu_M$	0.90(8)	1.19(13)		1.09(7)
$\beta_M/\nu_M$	0.44(5)?	0.56(10)?		0.58(14)?
$\gamma_M/\nu_M$	1.46(6)	1.46(18)		1.10(14)
$\alpha$	0 (log)	0 (log)	0 (log)	0

netic field [27]. In this case the exponents were reported to be nonuniversal (varying continuously with field strength). This might be the case here, but several points along the  $PQ_2$  would have to be done (with much better statistics) in order to follow the evolution of the critical exponents.

## V. CONCLUSION

We have presented the phase diagram of a model for columnar phases of HHTT in the limit of weakly interacting columns. Its Hamiltonian couples  $XY$  and Ising variables. We used the mean-field approximation, the Migdal-Kadanoff renormalization-group scheme, and Monte Carlo simulations. These techniques give qualitatively the same topology for the phase diagram, showing a phase with  $XY$  order and Ising disorder. Renormalization-group results and Monte Carlo simulations suggest that all the transitions are continuous. From the renormalization-group analysis, we found that the transition from phase III to phase II should be of the Ising type (Fig. 3). Preliminary Monte Carlo simulations on large lattice sizes are not inconsistent with this result and might

suggest that the transition from phase III directly to phase I is also of the 2D Ising universality class. (We emphasize, however, that our statistical errors appear to be quite large.) This latter result may be in disagreement with the suggestion by Granato *et al.* [15] of a new universality class.

*Note added.* After the original submission of this work we learned of Monte Carlo transfer-matrix calculations [31] that complement the works of Refs. [14–16].

## ACKNOWLEDGMENTS

We thank A. Caillé and A.M. Tremblay for useful discussions. One of the authors (M. H.) wishes to thank H.T. Diep for discussions on Monte Carlo simulations and acknowledge the hospitality of the Université de Cergy-Pontoise during the early stages of this work. This work was supported by the National Sciences and Engineering Research Council of Canada, the Fonds pour la Formation des Chercheurs et de l'Aide à la Recherche du Québec, and the Centre de Recherche en Physique du Solide.

- 
- [1] P.G. de Gennes and J. Prost, *The Physics of Liquid Crystals*, 2nd ed. (Oxford University Press, Oxford, 1993).
- [2] A. Caillé, M. Hébert, and M.L. Plumer, Phys. Can. **51** (5/6), 129 (1995).
- [3] D. Adam, P. Schummacher, J. Simmerer, L. Haussling, K. Siemensmeyer, K.H. Eitzbach, H. Ringsdorf, and D. Haarer, Nature **371**, 141 (1994).
- [4] B. Kohne, W. Poules, and K. Praefcke, Chem. Z. **108**, 113 (1984).
- [5] E. Fontes, Doctoral dissertation, University of Pennsylvania, 1989 (unpublished).
- [6] S.H. Idziak, Doctoral dissertation, University of Pennsylvania, 1992 (unpublished).
- [7] E. Fontes, P.A. Heiney, and W.H. de Jeu, Phys. Rev. Lett. **61**, 1202 (1988).
- [8] P.A. Heiney, E. Fontes, W.H. de Jeu, A. Reira, P. Carroll, and A.B. Smith III, J. Phys. (Paris) **50**, 461 (1989).
- [9] M. Gharbia, T. Othman, A. Gharbi, C. Destrade, and G. Durand, Phys. Rev. Lett. **68**, 2031 (1992); H.R. Brand and H. Pleiner, *ibid.* **69**, 987 (1992); G. Durand, *ibid.* **69**, 988 (1992).
- [10] A. Caillé and M. Hébert (unpublished).
- [11] M. Hébert and A. Caillé, Phys. Rev. E **53**, 1714 (1996).
- [12] M. Hébert and A. Caillé, Phys. Rev. E **51**, R1651 (1995).
- [13] M.L. Plumer, A. Caillé, and O. Heinonen, Phys. Rev. B **47**, 8479 (1993).
- [14] Jooyoung Lee, E. Granato, and J.M. Kosterlitz, Phys. Rev. B **44**, 4819 (1991), and references therein.
- [15] E. Granato, J.M. Kosterlitz, Jooyoung Lee, and M.P. Nightingale, Phys. Rev. Lett. **66**, 1090 (1991).
- [16] Jooyoung Lee, J.M. Kosterlitz, and E. Granato, Phys. Rev. B **43**, 11 531 (1991).
- [17] T. Horiguchi, D. Loison, H.T. Diep, and O. Nagai, Physica A **206**, 508 (1994).
- [18] G.H. Wannier, Phys. Rev. **79**, 357 (1950).
- [19] Mai Suan Li and Marek Cieplak, Phys. Rev. B **50**, 955 (1994).

- [20] B. Nienhuis, A.N. Berker, E.K. Riedel, and M. Schick, Phys. Rev. Lett. **43**, 737 (1979).
- [21] B. Nienhuis and M. Nauenberg, Phys. Rev. Lett. **35**, 477 (1975).
- [22] M. Yosefin and E. Domany, Phys. Rev. B **32**, 1778 (1985).
- [23] S. Fujiki and T. Horiguchi, J. Phys. Soc. Jpn. **64**, 1293 (1995).
- [24] M.L. Plumer, A. Caillé, A. Mailhot, and H.T. Diep, in *Magnetic Systems with Competing Interactions*, edited by H.T. Diep (World Scientific, Singapore, 1994).
- [25] P. Peczak, A.M. Ferrenberg, and D.P. Landau, Phys. Rev. B **43**, 6087 (1991).
- [26] K. Binder, Phys. Rev. Lett. **47**, 693 (1981).
- [27] D.H. Lee, J.D. Joannopoulos, and J.W. Negele, Phys. Rev. B **33**, 450 (1986).
- [28] M.L. Plumer and A. Mailhot, Phys. Rev. B **50**, 16 113 (1994).
- [29] J.N. Reimers, J.E. Greedan, and M. Björgvinsson, Phys. Rev. B **50**, 7295 (1992).
- [30] M.S.S. Challa, D.P. Landau, and K. Binder, Phys. Rev. B **34**, 1841 (1986).
- [31] M. P. Nightingale, E. Granato, and J. M. Kosterlitz, Phys. Rev. B **52**, 7402 (1995).